Applied Mathematics & Information Sciences
An International Journal

http://dx.doi.org/10.12785/amis/091L12

Interactive Medical Augmented Reality System for Remote Surgical Assistance

Tzyh-Chyang Chang[1,2], *Chung-Hung Hsieh*[1], *Chung-Hsien Huang*[1,3], *Ji-Wei Yang*[1], *Shih-Tseng Lee*[4,5], *Chieh-Tsai Wu*[4,5] *and Jiann-Der Lee*[1,*]

[1] Department of Electrical Engineering, Chang Gung University, Taoyuan, Taiwan
[2] Bali Psychiatric Center, Department of Health, Executive Yuan, New Taipei City, Taiwan
[3] Information& Communications Research Laboratories, Industrial Technology Research Institute, Hsinchu, Taiwan
[4] Department of Neurosurgery, Chang Gung Memorial Hospital, Taoyuan, Taiwan
[5] Augmented Reality Research Center, Chang Gung Memorial Hospital, Taoyuan, Taiwan

Received: 13 Nov. 2013, Revised: 14 Mar. 2014, Accepted: 15 Mar. 2014
Published online: 1 Feb. 2015

Abstract: Medical surgery is considered as a difficult technique and needs to be performed by well-trained and experienced medical personnel to complete the procedure. During a complicated surgery, an experienced surgeon at distant can provide sophisticated instruction or guidance to help the operating surgeon when it is necessary. In this study, we have designed an interactive augmented reality system for remote surgical assistance. The surgeon at the remote site can indicate or contour a region of interest (ROI) by manually drawing on streaming images which were captured by the camera at the local site. The coordinate of the ROI in the 3-D physical space can be estimated by using the CT images of the patient. Therefore, the ROI and the anatomical information of the CT images can be rendered on the captured images, overlaid on the patient and projected onto a head-mounted display of the local operating surgeon, providing an across-space augmented reality visualization.

Keywords: Medical Augmented Reality, Remote Surgical Assistance, Head-Mounted Display

1 Introduction

Performing medical surgery usually requires a lot of experiences and many complicated technical skills. Failure in an operation may cause the recurrence or death of the patient. With the advancement in the field of medical surgery, Image-Guided Surgery (IGS) has become an important part of medical surgery. Pre-operative medical images such as Computed Tomography (CT), Magnetic Resonance Imaging (MRI) or Ultrasound Image (US) were registered to the real position of patient. By using the techniques of augmented reality (AR) visualization [1], the registered medical images can be overlaid on the real space and help surgeons to verify the position of important targets.In medical AR system, information of anatomical interest, such as tumor or bone, is extracted from the registered medical images, represented as a graphical object, and then overlaid over a view of the real environment of the observer. With the combined view on the physical space and the medical imaging data, AR visualization can provide perceptive advantages. Usually a movable camera is used to record the physical world and the graphical object is rendered on the captured video frames, enriching the captured real surroundings of the observer. Therefore, medical AR can help medical doctors to reduce the difficulty of finding mentally corresponding regions in the image space and on the patient.

During a complicated surgery, even with the help of AR visualization, unpredictable situation usually happens. Sometimes it requires a professional and experienced surgeon to make some guidance or decision at that very moment. But most of the time, maybe the experienced surgeon is not in the place to provide the helpful assistance. If the expert surgeon, who is not in the place, can assist or guide the local surgeon during the surgery immediately, it would be a great help for the progress of medical surgery.

As stated above, development of remote surgical assistance has its necessity [2]. It can also be applied to

* Corresponding author e-mail: jdlee@mail.cgu.edu.tw

different fields of surgery [3,4,5]. Remote surgical assistance interchanges audio and visual information between a remote surgeon and the local surgeon. In [6], it mentions the concepts of interactive remote surgery. Due to the assistance of remote surgeon and the AR display at the local site, the success rate of the operation can be increased.

In traditional remote instruction, surgeons at the remote site only select a region of interest (ROI) on the images, which was captured and sent by the camera at local site. After the ROI selection of the remote-site doctor, the 2-D information of the ROI will be sent back to the local site. Because of the viewpoint of the local site may be changed, the 2-D information of ROI could not be project on the camera image in the right position. To deal with this problem, we propose a method to calculate the 3-D position of the selected ROI and apply it for AR display in this study. Basically, this method utilizes the line of vision of local-site camera and pre-registered medical images to reach the goal. In addition, a marker-less AR visualization was also implemented to integrate the pre-operative medical image with the real position of patient. The 3-D information of selected ROI can be displayed on the local camera image even with the viewpoint of local-site surgeon changes.

This paper is organized as follows. The framework of the proposed system and the details of its components are described in section 2. Experimental results and discussions are revealed in section 3. Finally, the conclusions and future works are revealed in section 4.

2 Methods

The main purpose of the proposed system is to construct a platform that the remote surgeon can give some instruction or guidance to the local surgeon. In addition, the provided guidance can be seen through an AR display at the local site. Fig. 1 shows the scenario for its applications. If the local surgeon needs some guidance, the system sends live video streaming to the remote site. The video is captured by a camera fixed on a head-mounted display (HMD) and the HMD is worn by a surgeon at local site. Therefore, the remote surgeon can provide surgical guidance or instruction by selecting some ROIs on the screen manually and send it back to the local site.

The flowchart of the proposed system is shown in fig. 2. This interactive remote AR system can be divided into two parts: the local and the remote site. The local site is at the location where surgeons perform operation. The remote site can let surgeons at distant to offer surgical assistance or guidance.

The remote site receives streaming video from the local camera. ROI can be selected on a video image, and the 3-D position of the ROI is then calculated by using the extrinsic parameters of the local camera and the pre-operative CT images of the patient.

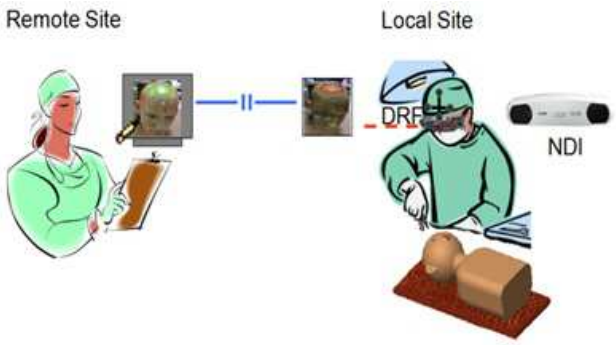

Fig. 1: Application scenario of the proposed system

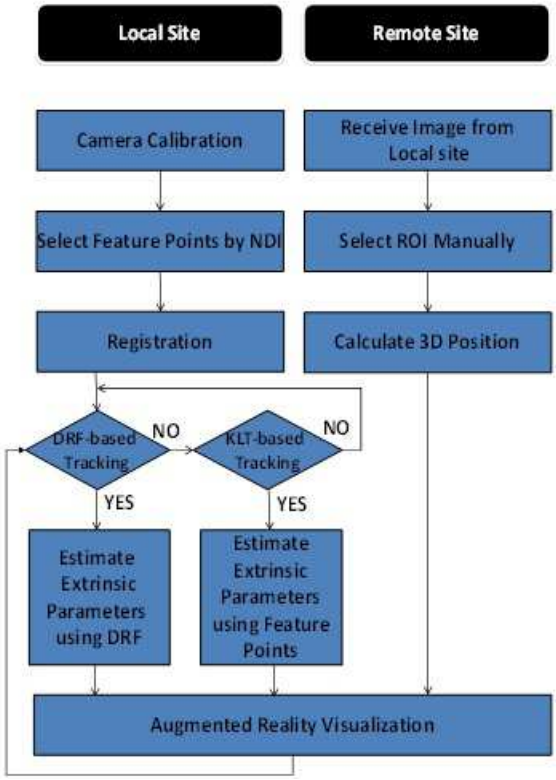

Fig. 2: Flowchart of the proposed AR remote surgical assistance system

At the local site, operating scene is captured by using a pre-calibrated camera which is fixed on a HMD. In order to perform AR display, position and posture of the camera should be known. A commercial spatial digitizing device named NDI POLARIS Vicra [7] is utilized herein to track a dynamic reference frame (DRF) installed on the HMD. The DRF is formed with four spherical, retro-reflective markers that reflect infrared light emitted by the illuminators on the position sensor of the NDI system. Since the detection range, related to the field of

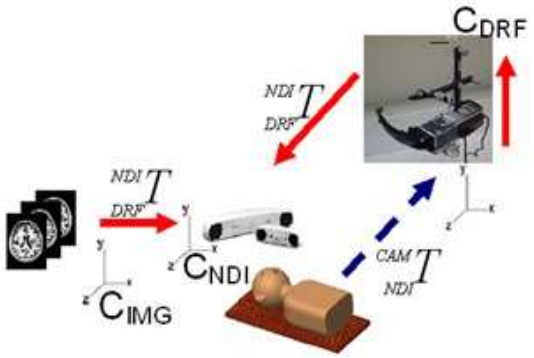

Fig. 3: Relationship of the coordinate systems

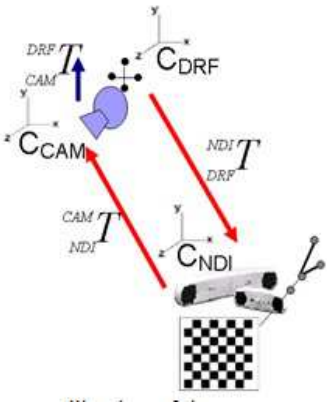

Fig. 4: Calibration of the AR camera

view (FOV) of the POLARIS Vicra, is limited, the proposed system uses Kanade-Luzas-Tomosi (KLT) [8] tracking method to track some pre-selected feature points when the DRF-based tracking is failed. However, if the KLT-based tracking fails, the proposed system needs to ask to the user to move back to the FOV of the POLARIS Vicra to re-initialize the DRF tracking. Last, the AR visualization provides the fusion images by overlaying the registered pre-operative CT images and the ROI on the patient in the operating scene.

2.1 Transformation of the Coordinate Systems

Four coordinate systems are involved in the proposed system comprises the NDI POLARIS Vicra C_{NDI}, the pre-operative CT images C_{IMG}, the HMD camera C_{CAM}, and the DRF C_{DRF}. Relationships among these four coordinate systems are shown in fig. 3.

In order to perform the AR visualization, the coordinate systems of the devices and the pre-operative CT images should be integrated together in the same coordinate system. Relationships among these transformations are revealed in Eq. (1). When the camera moves, the transformation ${}^{CAM}_{NDI}T$ between the coordinate system of the physical space, which was set as the coordinate of the POLARIS Vicra system, and the camera coordinate system is needed to be estimated in order to project the 3-D object onto the camera image.

$$ {}^{CAM}_{NDI}T = {}^{DRF}_{CAM}T^{-1} \times {}^{NDI}_{DRF}T^{-1} \tag{1} $$

2.1.1 Transformation between C_{IMG} and C_{NDI}:

Before taking the pre-operative CT images, some skin markers need to be attached on the patient as references for CT/patient registration. Assume there are N markers and these markers can be easily recognized on the CT images. Their 3-D coordinates in the CT coordinate system are denoted as $P_{CT}\{m_1, m_2, , m_N\}$. On the other hand, we use spatial digitizing devices, i.e., NDI POLARIS Vicra herein, to get the 3-D coordinates $P_{NDI}\{n_1, n_2, , n_N\}$ of these markers too. By using Eq. (2), the transformation ${}^{NDI}_{CT}T$ between C_{IMG} and C_{NDI} can be calculated by using Least Squares Method (LSM) [9].

$$ P_{NDI} = {}^{NDI}_{CT}T \times P_{DRF} \tag{2} $$

2.1.2 Transformation between C_{DRF} and C_{NDI}:

Since the DRF is installed on the HMD with camera, we can get ${}^{NDI}_{DRF}T$ directly by using NDI POLARIS Vicra to track the DRF.

2.1.3 Transformation between C_{CAM} and C_{DRF}:

Because that the DRF is attached on the HMD with camera, the relationship between C_{CAM} and C_{DRF} is fixed. As a result, the transform ${}^{DRF}_{CAM}T$ can be obtained by a calibration step, as shown in fig. 4.

The calibration step is described as below: At first, the POLARIS Vicra is utilized to get the 3-D coordinates of corner points $P_{NDI}\{n_1, n_2, , n_N\}$ of a chessboard-like pattern. The corners can be tracked on the images captured by the moving camera, and the extrinsic parameter ${}^{CAM}_{NDI}T$ of the camera can thus be calculated. By using the POLARIS Vicra to track the DRF, we can get ${}^{NDI}_{DRF}T$. According Eq. (3) and Eq. (4), P_{NDI} can be transformed to C_{CAM} and C_{DRF}. Finally, the transformation ${}^{DRF}_{CAM}T$ can be estimated by using Eq. (5).

$$ P_{CAM} = {}^{CAM}_{NDI}T \times P_{NDI} \tag{3} $$

$$ P_{DRF} = {}^{NDI}_{DRF}T \times P_{NDI} \tag{4} $$

$$ P_{DRF} = {}^{DRF}_{CAM}T \times P_{CAM} \tag{5} $$

2.1.4 Transformation between C_{CAM} and C_{DRF}:

Because the FOV of the POLARIS Vicra is limited, when the DRF tracking fails, ${}^{CAM}_{NDI}T$ cannot be calculated properly by using Eq. (1). Therefore, the tracking procedure was considered in two situations: The DRF has been tracked or The DRF tracking failed. If the system can track the DRF, we will have the transformation ${}^{NDI}_{DRF}T$ between coordinate system C_{DRF} and C_{NDI}. With the transformation ${}^{DRF}_{CAM}T$ which is obtained by the calibration step, ${}^{CAM}_{NDI}T$ can be calculated by using Eq. (1), and the AR visualization can be performed. If occlusion happens and the DRF tracking fails, the proposed system uses KLT algorithm to track some feature point whose 3-D coordinates are obtained by using the probe of the POLARIS Vicra beforehand. The KLT tracking algorithm takes horizontal and vertical intensity gradient of a pixel to calculate covariance matrix, and uses covariance matrix to determine whether this pixel is a tracking feature should or not. With 3-D coordinates of these feature point, 2-D image points which are tracked by KLT, and intrinsic parameters of the camera, we can calculate the extrinsic parameters of the camera ${}^{CAM}_{NDI}T$ by using Eq. (6).

$$\begin{bmatrix} x_n \\ y_n \\ s \end{bmatrix} = \begin{bmatrix} f_x & 0 & c_x \\ 0 & f_y & c_y \\ 0 & 0 & 1 \end{bmatrix} \times \begin{bmatrix} R_1 & R_2 & R_3 & T_x \\ R_4 & R_5 & R_6 & T_y \\ R_7 & R_8 & R_9 & T_z \end{bmatrix} \times \begin{bmatrix} X_n \\ Y_n \\ Z_n \\ 1 \end{bmatrix} \quad (6)$$

where s is a ratio of image scaling. (x_n, y_n) are the coordinates of the feature point on the camera image. f_x, f_y, C_x and C_y are intrinsic parameters of the AR camera, and they stands for camera focus and image center, respectively. $\begin{bmatrix} \boldsymbol{R} & \boldsymbol{T} \end{bmatrix}_{3\times4}$ are extrinsic parameters of the AR camera. (X_n, Y_n, Z_n) are 3-D coordinates of feature points which are obtain by the probe of the POLARIS Vicra.

2.2 Calculating 3-D Coordinates of ROI

The remote surgeon can select an ROI on the streaming video, which is captured from the local-site AR camera. Because of the viewpoint of local-site camera will change, the ROI which is selected from image of the 2-D camera will not be on the right place if the camera is moved. Here we will explain how to reconstruct the 3-D coordinates of the ROI from the remote-selected 2-D ROI.

At first, by applying a user-defined threshold of Hounsfield value, we can separate the pre-operative CT into head region and background region. The first outer contour of the head region can be found by using a chain-code-based contour detection algorithm to obtain the facial point cloud from the pre-operative CT images. The contour detection algorithm applied herein was obtained from the Intel OpenCV library [10]. By using Eq. (2), the coordinates of CT point cloud can be changed

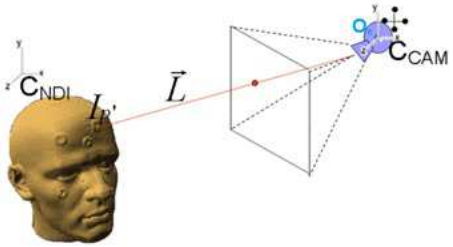

Fig. 5: ROI 3-D reconstruction using camera line of vision

to the coordinate system of NDI. Assuming a 2-D point on the image captured by the camera, by using the intrinsic and extrinsic parameters of the camera, we can calculate a vector L from the origin of camera O_c to the surface of the object, which can be represented as Eq. (7). Because of the 3-D point which projects this image point must be on the line, we search in the CT point cloud to find several points I_p whose distance from L is below a threshold h, as shown in Eq. (8). The notation t is a scaling factor, and p stands for a point in CT point cloud. However, this criterion may find several candidate points.

By applying Eq. (1), we can change these points to the camera coordinate system and pick up the point $I_p^{'}$ which is the closet point to O_c. We assign this point $I_p^{'}$ as the 3-D point of this image point. This method is illustrated in fig. 5.

$$L = O_c + \rightarrow Lt \quad (7)$$

$$I_p^{'} = \arg\min d(I_p, O_c), if d(\boldsymbol{p}, L) < h \quad (8)$$

2.3 Network Transmission

The network transmission of the proposed system is established on a simple point-to-point data streaming based on TCP-IP protocol. The video stream captured by local-site camera is sent to the remote site, and the remote site locates an image buffer to receive the streaming images. Intuitively, after the remote site selects the ROI and sends this information back to local, 3-D coordinates of the ROI will be computed at the local site. However, this data sending approach suffers the problem of synchronization. In other words, frames seen by the remote-site surgeon will keep changing because the local camera is not always at the same place. Our system has a simple mechanism to solve this synchronization problem. When the remote-site surgeon starts selecting ROI, the image on the remote screen will be fixed and the extrinsic parameters of the local-site camera at this moment will be recorded. After ROI selection complete, 3-D coordinates of ROI will be computed by using the recorded camera posture.

(a)

(b)

(c)

Fig. 6: AR display (a) when DRF tracking is available (b) when DRF tracking is failed and instead by using KLT tracking (c) another view when DRF tracking is available

3 Experimental Results

The proposed system utilized Microsoft Visual Studio 2008 as development platform, and was implemented by C++ language with three open source libraries, OpenCV, ARToolKit [11] and OpenGL [12]. The HMD device used here is Iwear-VR920 from VUNIX Inc., which is integrated with a webcam and a DRF. The image resolution of the webcam is 640 x 480.

A plastic phantom, as shown in fig. 6 (a), was used to demonstrate and evaluate the proposed system. Five skin markerswere attached to the phantombefore CT scans so they can be utilized for CT /patient registration.

First, an example shown in fig. 6 is used to demonstrate the DRF-based tracking and the KLT-based tracking. When DRF is detected by the POLARIS Vicra, the 3-D model, which is reconstructed from the pre-operative CT image, will be projected onto the image captured by the AR camera through the extrinsic parameters calculated by DRF detection, as shown in fig. 6. The yellow points in fig. 6(a) represent the 2-D feature points which are projected by using extrinsic parameters, which are estimated by using the DRF detection. When DRF tracking is out of FOV, the KLT-based tracking is utilized to track these 2-D feature points. Since the 3-D positions of these 2-D points are known, the tracked feature points (green points) can thus be utilized to compute the extrinsic parameters, as shown in fig. 6 (b). Fig. 6(c) illustrates another view when DRF tracking is available again.

Fig. 7: ROI selection at remote site

Fig. 7 shows an example when a remote surgeon selects a ROI on the image, which was sent from the local camera. The coordinates of the pixels on the selected ROI are then sent back to the local site, and the 3-D coordinates of the ROI will be computed by using Eq. (7) and Eq. (8). The AR visualization of the selected ROI and the reconstructed CT surface at local-site screenare shown in fig. 8 (a). In fig. 8(b), we can see that even the viewpoint of local-site is changed, the ROI can still be projected at the right position.

Last, the accuracy of the AR alignment was evaluated. As shown in fig. 9, eight feature points which are localized by the probe of POLARIS are utilized here as gold standard, compared with the eight 3-D points which the proposed system reconstructed. The target registration error (TRE) was computed by estimating the Euclidean distance between the corresponding points. The camera was placed at different distances, ranged from 30 50 cm, away the object with different view angels, which were ranged from -60 to 60 to evaluate the registration errors, as shown in fig. 10. Fig. 11 shows the images captured by the AR camera at different locations and view angels.

Table 1, table 2 and table 3 shows the results of TRE estimation when the camera was placed at 30, 40 and 50 cm, respectively. The notation N/A stands for either that the target points was invisible caused by self-occlusion or that the DRF was out of range of the NDI detector.

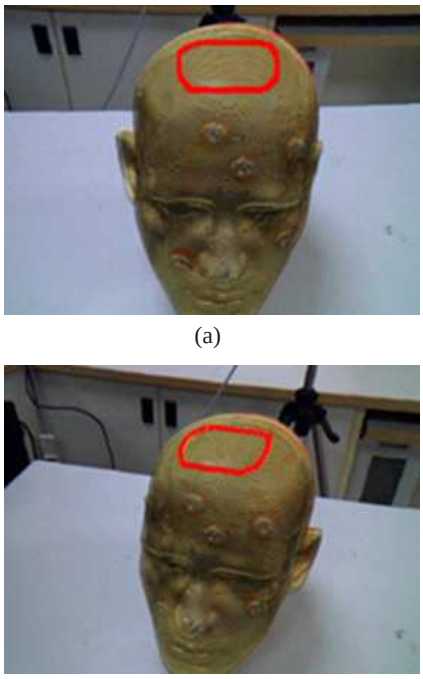

(a)

(b)

Fig. 8: (a) AR visualizationof the selected ROI and the reconstructed CT images (b) observation from another viewpoint

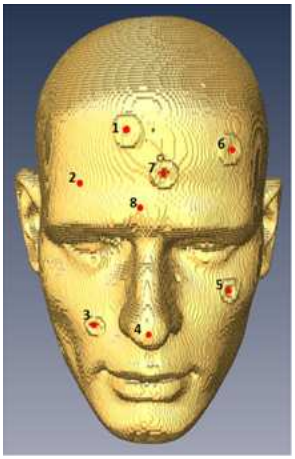

Fig. 9: Accuracy evaluation on AR display

From the results in these tables, although the TREs seem slightly smaller when the camera is at zero degree, it does not show significant different from the other angels. In addition, the distance factor of placing the AR camera does not affect the accuracy of registration too. It means that when the system is operated within the FOV of the POLARIS Vicra tracking system, the error is consistently in the range of 3 ≈5 mm. The error may be

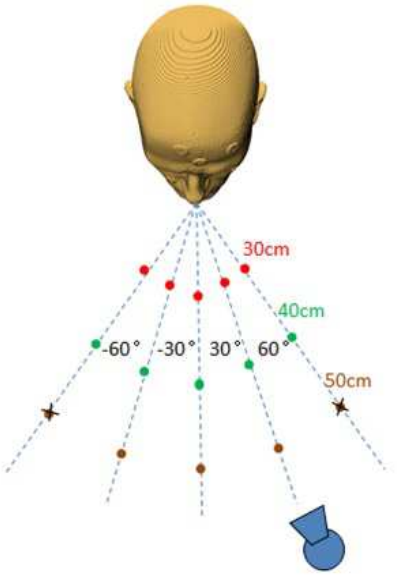

Fig. 10: The camera locations for accuracy evaluation of AR registration

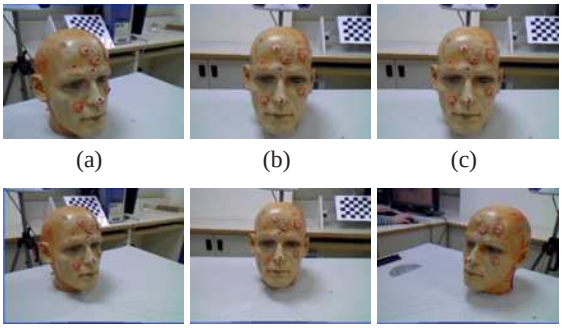

(a) (b) (c)

(d) (e) (f)

Fig. 11: Images captured when camera is at different location with different view angel. (a) 30cm, -30° (b) 30cm, 0° (c) 30cm, 30° (d) 40cm, -30° (e) 40cm, 0° (f) 40cm, 30°

Table 1: TREs when camera is placed 30 cm away from the phantom

	-60°	-30°	0°	30°	60°	Ave.
Point 1	3.89	2.48	2.26	3.9	5.33	3.57
Point 2	5.2	3.39	1.08	4.86	2.05	3.32
Point 3	3.76	3.55	4.11	6.22	N/A	4.41
Point 4	3.99	5.02	2.03	5.64	6.03	4.54
Point 5	N/A	4.59	3.92	2.6	1.54	3.16
Point 6	N/A	N/A	3.49	3.36	2.45	3.1
Point 7	2.94	1.79	2.01	2.59	2.77	2.42
Point 8	3.4	3.02	3.02	3.55	2.43	3.08
Ave.	3.86	3.4	2.74	4.09	3.22	

Table 2: TREs when camera is placed 40 cm away from the phantom

	-60°	-30°	0°	30°	60°	Ave.
Point 1	5.15	2.5	2.84	1.74	2.67	2.98
Point 2	5.13	3.1	3.56	0.99	6.5	3.85
Point 3	3.8	2.62	4.13	4.94	N/A	3.87
Point 4	3.16	6.9	3.84	5.73	6.58	5.2
Point 5	N/A	4.45	2.63	2.84	2.84	2.98
Point 6	N/A	N/A	3.23	2.99	2.31	2.84
Point 7	3.8	4.98	2.8	3.78	2.1	3.49
Point 8	5.15	4.71	4.12	2.82	2.3	3.82
Ave.	4.36	4.18	3.39	3.22	3.4	

Table 3: TREs when camera is placed 50 cm away from the phantom

	-60°	-30°	0°	30°	60°	Ave.
Point 1	N/A	2.04	2.39	2.01	N/A	2.15
Point 2	N/A	2.29	2.55	3.7	N/A	2.85
Point 3	N/A	2.79	3.4	5.8	N/A	3.99
Point 4	N/A	6.44	2.69	5.7	N/A	4.94
Point 5	N/A	5.14	4.28	3.54	N/A	4.32
Point 6	N/A	N/A	4.08	3.75	N/A	3.91
Point 7	N/A	2.77	2.71	2.51	N/A	2.66
Point 8	N/A	4.27	4.35	4.19	N/A	4.27
Ave.	N/A	3.67	3.3	3.9	N/A	

(a) (b)

Fig. 12: Example to demonstrate the AR visualization on a person

caused by the CT/patient registration or ${}^{CAM}_{NDI}T$ estimation in the step of AR camera calibration.

Last, we applied the AR function of the proposed system on a real person. The results of AR visualization at different viewpoints are shown in fig. 12 (a) and (b). The sagittal plane of CT is overlaid on a testing person and the red spot is an interest target indicated from remote site. When the help of AR visualization, the proposed system provides spatially coherent anatomical information to observers and is expected for applying on other potentially medical applications.

4 Conclusions and Future Works

In this paper, we have designed an interactive AR system for remote surgical assistant, which can also be applied on surgery training. Remote-site surgeons can manually draw an ROI on the streaming video and then send their assistance or guidance back to the local site. In addition, the pre-operative medical images can also be fused on real camera scene with the ROI indicated from the remote site to perform an AR display. So far, the AR registration error is ranged from 3≈5 mm and it may be too large to satisfy some high-accuracy-demand medical applications. The first priority in our future works will be focused on raising the accuracy of AR registration. Furthermore, the operation range of the proposed system is still constrained by the FOV the POLARIS Vicra. Applying another spatial tracing hardware or developing pure computer-vision tracking algorithm is under consideration to breaking this limitation.

Acknowledgement

This study is supported by the technology development program of Ministry of Economic Affairs, R. O. C. (serial number: 99-EC-17-A-19-S1-035)
The authors are grateful to the anonymous referee for a careful checking of the details and for helpful comments that improved this paper.

References

[1] H. Kato and M. Billinghurst, Proceedings of 2nd IEEE and ACM International Workshop on Augmented Reality, **3**, 85-97 (1999)
[2] P. Whitten and F. Mair, Surgery Technology International, **12**, 68-72 (2004)
[3] J. Marescaux, J. Leroy, F. Rubino, M. Smith, M. Vix, M. Simone, and D. Mutter, Annals of Surgery, **235**, 487-492 (2002)
[4] M. Larkin, the Lancet, **358**, 1074 (2001)
[5] P. Bove, D. Stoianovici, S. Micali, A. Patriciu, N. Grassi, T. Jarrett, G. Vespasiani, and L. Kavoussi, Journal of Endourology, **17**, 137-142 (2003)
[6] M. Shenai, M. Dillavou, C. Shum, D. Ross, R. Tubbs, A. Shih, and B. Guthrie, Neurosurgery, **68**, 200-207 (2011)
[7] Northern Digital Inc., http://www.ndidigital.com.
[8] C. Tomasi and T. Kanade, Carnegie Mellon University Technical Report, CMU-CS-91-132 (1991)
[9] W. Donald, Journal of the Society for Industrial and Applied Mathematics, 431-441 (1963)
[10] Open Computer Vision Library, OpenCV, http://sourceforge.net/projects/opencvlibrary/
[11] Artoolkit, http://www.hitl.washington.edu/artoolkit/
[12] Open Graphic Library, OpenGL, http://www.opengl.org/

Tzyh-Chyang Chang received his M. A. degrees in 1998 from New York University, New York, USA. Now he is a Ph.D student of Department of Electrical Engineering of Chang Gung University. He is now a director of Department of Occupational Therapy, Bali Psychiatric Center, Taiwan. His research interests include medical image processing, telemedicine and medical informatics.

Chung-Hung Hsieh received the B.E.E and M.S degree in 2007 and 2010 from Chang Gung University. Now he is a Ph.D student of Electrical Engineering of Chang Gung University. His research interests include medical image processing, computer vision and augmented reality.

Chung-Hsien Huang received his B. E. E., M. S. and Ph. D. degrees in Electrical Engineering in 1998, 2000 and 2007 respectively from Chang Gung University, Taiwan. He is now a researcher working with the Information & Communications Research Laboratories at the Industrial Technology Research Institute. His research interests include medical image processing, computer vision and pattern recognition.

Ji-Wei Yang received the B.E.E degree in 2009 from Chung Hua University. Now is a Master student of Chang Hung University. His research interests include medical image processing, computer vision and augmented reality.

Shih-Tseng Lee received his M.D. from Taipei Medical College, Taipei, Taiwan, Republic of China, in 1978. He currently is on the faculty of the Medical School of Chang Gung University. He is also Professor of Neurosurgery in Chang Gung Memorial Hospital and Chang Gung University.

Chieh-Tsai Wu received his M.D. from Taipei Medical College, Taipei, Taiwan, Republic of China, in 1989. He currently is on the faculty of the Medical School of Chang Gung University. He is also the chief of the Division of neuro-trauma and neuro-critical care in Department of Neurosurgery of Chang Gung Memorial Hospital and Chang Gung University.

Jiann-Der Lee received his Ph.D. degrees in Electrical Engineering from National Cheng Kung University, Taiwan, Republic of China, in 1992. Since then he has been on the faculty of Chang Gung University, where he is currently full professor and chairman in the department of Electrical Engineering. During the past five years, he has received a number of investigator awards (e.g. from National Science Council and Acer Foundations). Besides, he received the Excellent Teaching Award, 2002, and the Excellent Research Award, 2003, from the Chang Gung University. He is a member of IEEE and IAPR, and is listed in the Whos Who in the World, Who's Who in Finance and Industry. His current research interests include medical image processing, pattern recognition, computer vision, consumer electronics and VLSI CAD design. He has published over 60 journal papers and given more than 50 technical presentations at meetings of professional societies.